ELSEVIER

Materials Science and Engineering A270 (1999) 183–189

MATERIALS SCIENCE & ENGINEERING A

Nonequilibrium microstructures and their evolution in a Fe–Cr–W–Ni–C laser clad coating

Xiaolei Wu *, Guangnan Chen

Laboratory for Nonlinear Mechanics of Continuous Media, Materials Research Center, Institute of Mechanics, Chinese Academy of Sciences, Beijing 100080, Peoples Republic of China

Received 25 September 1998; received in revised form 30 March 1999

Abstract

The laser-solidified microstructural and compositional characterization and phase evolution during tempering at 963 K were investigated using an analytical transmission electron microscope with energy dispersive X-ray analysis. The cladded alloy, a powder mixture of Fe, Cr, W, Ni, and C with a weight ratio of 10:5:1:1:1, was processed with a 3 kW continuous wave CO_2 laser. The processing parameters were 16 mm/s beam scanning speed, 3 mm beam diameter, 2 kW laser power, and 0.3 g/s feed rate. The coating was metallurgically bonded to the substrate, with a maximum thickness of 730 μm, a microhardness of about 860 Hv and a volumetric dilution ratio of about 6%. Microanalyses revealed that the cladded coating possessed the hypoeutectic microstructure comprising the primary dendritic γ-austenite and interdendritic eutectic consisted of γ-austenite and M_7C_3 carbide. The γ-austenite was a non-equilibrium phase with extended solid solution of alloying elements and a great deal of defect structures, i.e. a high density of dislocations, twins, and stacking faults existed in γ phase. During high temperature aging, in situ carbide transformation occurred of M_7C_3 to $M_{23}C_6$ and M_6C. The precipitation of $M_{23}C_6$, MC and M_2C carbides from austenite was also observed. © 1999 Elsevier Science S.A. All rights reserved.

Keywords: Laser surface cladding; Microstructure; Phase transformation; Carbide

1. Introduction

Laser surface cladding or alloying associated with a rapid heating and cooling rate provided a unique opportunity for the non-equilibrium synthesis of materials and produced rapidly solidified fine microstructures with extended solid solution of alloying elements. The potential of such techniques was demonstrated for Fe-, Co-, and Ni-based alloy coatings synthesized on various substrate materials. Therefore, the microstructures by laser cladding or alloying can be described as in situ composites. With proper selection of alloying elements and processing parameters, materials could be synthesized with tailored properties such as corrosion and wear resistance [1–3].

Tailor-made coating materials produced by means of laser surface alloying and cladding techniques were researched. The formation of uniformly sized M_7C_3 carbides was identified in steels by laser alloying with a Cr–C powder mixture [4]. Wear testing and characterization of a laser-cladded powder mixture composed of Cr–Ni–Mo and Cr-carbides revealed wear resistance superior to that of a plasma-sprayed coating having a similar composition, good interfacial adherence, and a uniform microstructure consisting of molybdenum dendrites surrounded by a chromium–nickel matrix containing chromium carbides [5]. Singh and Mazumder [6] revealed wear properties of laser clad Fe–Cr–Mn–C alloys to be superior to Stellite 6 with metastable M_6C and M_7C_3 carbide precipitates. Nagarathnam and

Table 1
Size and purity of clad powders

Element	Fe	C	Cr	W	Ni
Purity (wt.%)	99.70	99.99	98.70	99.50	99.97
Size (μm)	40	28	40	60	40
Content (wt.%)	55.56	11.11	11.11	11.11	11.11

* Corresponding author. Tel.: +86-10-625-61284; fax: +86-10-625-47527.

E-mail address: xlwu@cc5.imech.ac.cn (X. Wu)

0921-5093/99/$ - see front matter © 1999 Elsevier Science S.A. All rights reserved.
PII: S0921-5093(99)00159-8

Table 2
Chemical composition (wt.%) of 5CrMnMo substrate

C	Cr	Mn	Mo	Si	P	S	Fe
0.52	1.21	1.18	0.33	0.25	<0.018	<0.035	Bal.

Komvopoulos [7,8] showed a very fine duplex cladding microstructure of fine-grained austenite matrix with carbide precipitates of Fe–Cr–W–C alloys with good resistance against shear deformation and microcracking. Microstructural characterization of laser-alloyed Fe–C–Cr system demonstrated the formation of a fully martensitic phase with dislocated lath-type substructures and twinned austenite needles or $M_{23}C_6$ carbides in a dislocated ferrite matrix, depending on the concentration of Cr [9]. With a similar Fe–Cr–C ternary system, refined microstructures possessing metastable crystalline and amorphous phase were reported for laser surface alloying [10].

The present investigation analyzed the crystal structures and microchemistry of phases under optimum process conditions and tracked systematically microstructural evolution during tempering in the clad coating.

2. Experimental procedure

The coating alloy was a powder mixture of Fe, Cr, W, Ni and C with a weight ratio of 10:5:1:1:1. The size and purity of element powders are shown in Table 1. The substrate material was a 5CrMnMo steel and its composition is given in Table 2. Rectangular specimens, 10 cm long, 4 cm wide, and 1.5 cm thick, were austenized at 1153 K × 20 min, oil cooled, and then tempered at 833 K × 60 min.

Laser surface cladding was carried out using a continuous wave 3 kW CO_2 laser equipped with a powder delivery system and an argon gas guidance device. The laser parameters in the present investigation were: 16 mm/s beam scanning speed, 3 mm beam diameter, 2

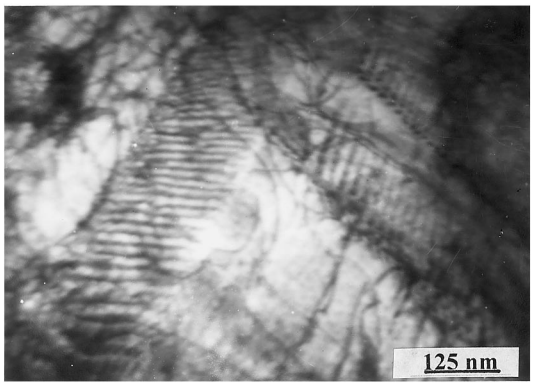

Fig. 2. TEM bright-field image showing a high density of dislocations of primary γ-austenite.

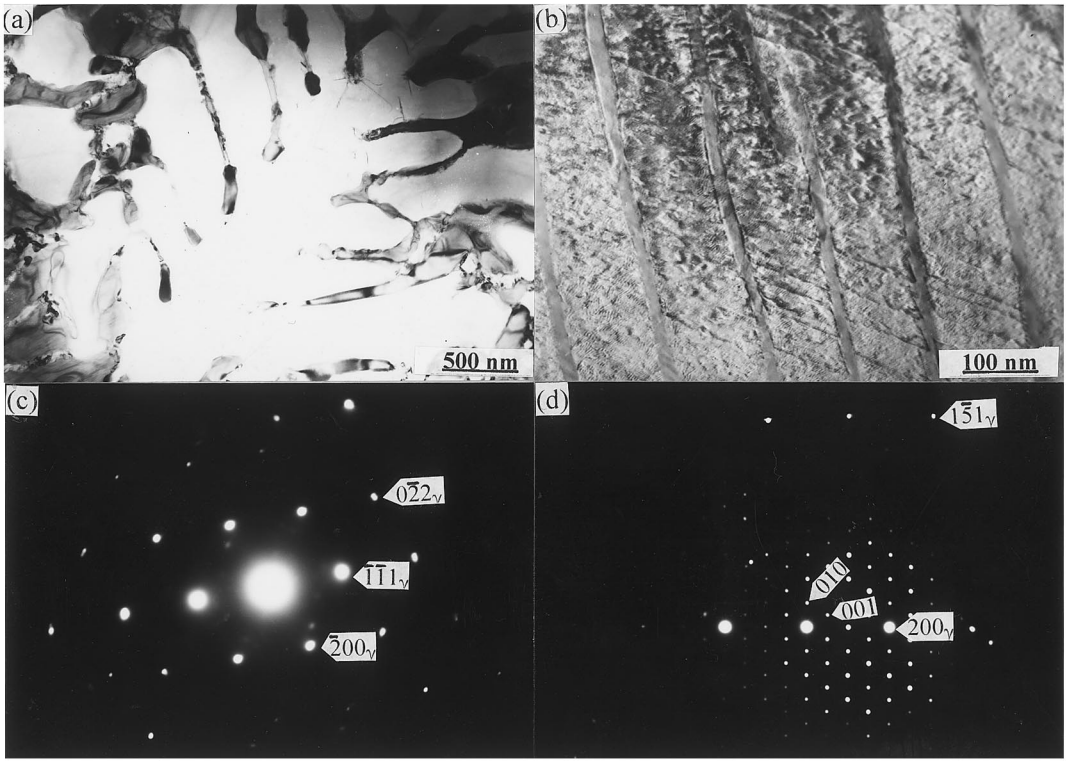

Fig. 1. TEM micrographs showing the laser-clad microstructure of the coating: (a) bright-field image of the primary dendritic γ-austenite; (b) bright-field image of the lamellar eutectic consisting of γ-austenite and M_7C_3 carbide; (c) SADP of γ-austenite in (a) with zone axis [011]; (d) SADP of γ-austenite and M_7C_3 carbide in (b) with zone axes [015] and [100] respectively.

Table 3
Microchemistry data of phases in the as-cladded coating by TEM/EDX

Phase structure	Element content (mass.%)					Stoichiometry
	Cr	Fe	W	Ni	C	
Primary γ	11.54	82.56	1.48	3.73	1.29	
Eutectic γ	16.21	67.98	4.64	5.46	2.71	
M_7C_3	48.42	36.58	3.93	2.52	8.55	$Cr_{3.92}Fe_{2.75}W_{0.09}Ni_{0.18}C_3$

kW laser power, and 0.3 g/s feed rate. The coating metallurgically bonded to the steel substrate was obtained, with a maximum thickness of 730 μm, a volumetric dilution ratio of about 6%, and free from pores and cracks [11].

Both the as-solidified and the as-aged microstructures at 963 K for 1 h were analyzed using H-9000 and Philips EM420 analytical transmission electron microscope (TEM). Thin TEM slices, 0.2 mm in thickness, were taken using a slow-speed cut-off saw, parallel to the cladding surface and at a distance of 0.3 mm away from the top surface of the coating. Slices were then cut into 3-mm disks using an ultrasonic disk cutter. Disks were dimpled on both sides by a dimple grinder and subsequently ion milled at an angle of 10°, to perforation under a voltage of 5.5 kV. The chemical compositions of each phase were determined using energy-dispersive X-ray analysis (EDX) and an electron energy loss spectrometer (EELS) in conjunction with TEM. The electron beam of TEM EDX produced an electron spot of about 10 nm diameter.

X-Ray diffraction (XRD) was performed with a D_{max}-RB 12 kW diffractometer in a 2θ scan. The radiation was Co Kα with a wavelength, working voltage, current, and step speed of 0.178892 nm, 30 kV, 120 mA, and 5° min^{-1} respectively. A zirconium filter was used to minimize the effects of Kβ peaks.

Microhardness measurements were obtained with a Vickers hardness tester using a 0.2-kg load.

3. Results and discussion

3.1. As-solidified microstructures

Fig. 1(a,b) show TEM micrographs of the laser-clad coating. The primary dendritic phase is determined to be FCC structure γ-austenite, as shown in Fig. 1(a). Fig. 1(c) is its selected area diffraction pattern (SADP) with a zone axis [011]. Fig. 1(b) reveals the interdendritic lamellar eutectic composed of γ-austenite and M_7C_3 carbides and Fig. 1(d) is the corresponding SADP. Zone axes of both γ-austenite and M_7C_3 carbide are [015] and [100] respectively. Thus, the clad coating is of hypoeutectic microstructure. M_7C_3 carbides possess a pseudohexagonal close-packed (hcp) crystal structure and the unit cell dimensions are $a_0 = 1.3979$ nm and $c_0 = 0.4618$ nm.

Additionally, a large amount of defect structures, such as high dislocation densities, stacking faults, and twins, exist in the primary and eutectic γ-austenite, as shown in Fig. 2.

The cooling rates are generally inversely proportional to the spacing of the dendrite arms. For the range of spacings between primary dendrites in the clad coating shown in Fig. 1(a) and from results for cooling rates of similar Fe-based alloys [12,13], it may be postulated that the cooling rate is in the range of 10^3–10^5 K/s.

Table 3 shows the quantitative microchemistry of various phases determined by EDX and EELS. It can be seen that the γ-austenite is a nonequilibrium phase with extended alloy element content, consistent with previous experimental results [7,8]. M_7C_3 is a Cr-rich carbide. It is also noted that the contents of Cr, Ni, and W elements in both austenite and M_7C_3 carbides vary with the depth of the molten pool. From the lower to the upper zone of the clad coating, for example, the experimental values of tungsten contents in M_7C_3 is in a range from 1.24 to 5.68 wt.%.

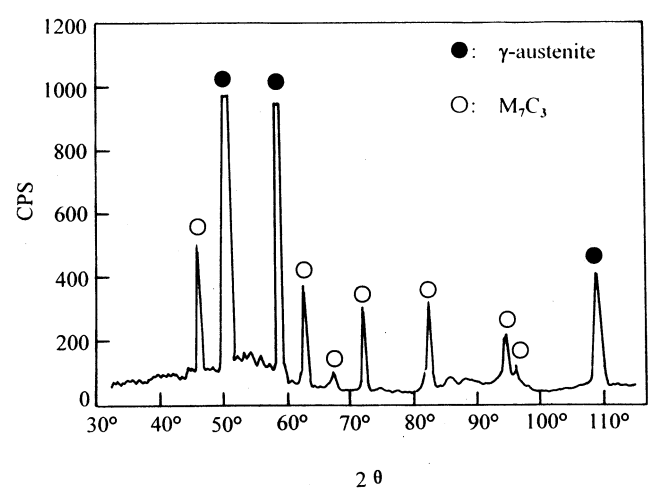

Fig. 3. X-Ray diffraction analysis of the as-cladded coating.

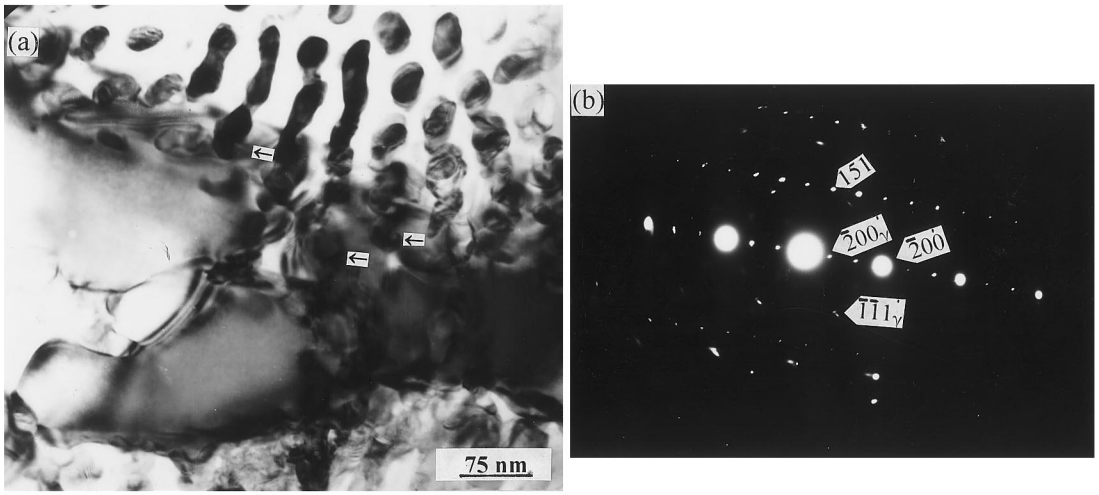

Fig. 4. TEM micrograph showing an in situ transformation of M_7C_3 to $M_{23}C_6$ carbide: (a) bright-field image; (b) SADP of $M_{23}C_6$ carbide and γ-austenite with zone axes [015] and [011] respectively (all the arrows indicate $M_{23}C_6$ carbides).

X-Ray diffraction analysis of the as-cladded coating is shown in Fig. 3. It is indicated that constituent phases of the cladded microstructure consist of γ-austenite and M_7C_3 carbides, consistent with TEM results. The volume fractions of austenite and M_7C_3 carbides are approximately 59 and 41% respectively. The estimated lattice parameter of austenite is in the range 0.3684–0.3696 nm, significantly higher than those obtained with conventional treatments by comparison of the experimentally determined *d* spacings with those given in the standard X-ray powder diffraction data. Therefore, the austenite is a nonequilibrium phase with extended alloy solubility. The existence of austenite is mainly attributed to the low martensite-start temperature, the high concentration of austenite stabilizing elements, and the rapid cooling rate, in agreement with the findings of other studies dealing with similar Fe-based alloys [7,8]. In addition, it has also been determined by TEM observation and X-ray diffraction analysis, that no bcc structure exists, such as δ-ferrite and martensite.

The hardness of the austenite matrix and hard carbide phases determines the overall hardness of the clad coating. Despite a large proportion of austenite, the hardness of the as-cladded coating is remarkably high, about 860 $Hv_{0.2}$. The hardness of M_7C_3 is about 1735 MPa [14]. The austenite is strengthened by the solid solution hardening due to W, Cr, and Ni, Orowan looping around impenetrable carbides, and dislocation–dislocation interactions.

3.2. Carbide evolution and precipitation

Carbide evolution and precipitation have been of great interest. The formation of carbides can take place either by in situ homogeneous mode within the pre-existing carbide or by a heterogeneous mode. The in situ transformation sequence $M_3C \rightarrow M_7C_3 \rightarrow M_{23}C_6 \rightarrow M_6C$ was established in chromium alloyed steels [15]. M_7C_3 is a metastable phase and as a result, its decomposition will occur during tempering. In addition, the precipitation of various carbides from nonequilibrium austenite is also thermodynamically favorable.

Fig. 4(a) is a TEM micrograph revealing in situ transformation of eutectic M_7C_3 to $M_{23}C_6$ carbides. M_7C_3 and fine spherical $M_{23}C_6$ carbides possess a light and dark black contrast respectively. $M_{23}C_6$ carbides are found to nucleate either within M_7C_3 or at the M_7C_3 and austenite interface, as indicated by arrows. In the case of tempering for a long time or at an even high temperature, $M_{23}C_6$ carbides grow and then M_7C_3 carbides disappear. Thus, the decomposition of M_7C_3 can be expressed as $M_7C_3\ (+\gamma) \rightarrow M_{23}C_6$. Fig. 4(b) is SADP taken from $M_{23}C_6$ carbides and surrounding austenite matrix, with zone axes [015] and [011] respectively. $M_{23}C_6$ is determined by EDX to be a Cr–Fe-rich carbide with stoichiometry of $Cr_{11.94}Fe_{10.76}W_{0.12}Ni_{0.18}C_6$.

Fig. 5(a,b) are TEM bright-field images revealing an in situ transformation of M_7C_3 to M_6C carbides. Both the lamellar and large granular carbides are M_7C_3 with a light black contrast. Fine granular carbides with a dark black contrast are determined to be M_6C-type carbides. Fig. 5(c) shows SADP taken from an area covering M_7C_3 carbides with a zone axis [100] in Fig. 5(a). Fig. 5(d) shows SADP taken from an area covering M_6C carbides and the surrounding austenite matrix with zone axes [110] and [010] respectively in Fig. 5(a). It is observed that M_6C carbides indicated by arrows nucleate at M_7C_3/austenite interfaces. Thus, the formation of M_6C carbides may be described as $M_7C_3 + \gamma \rightarrow M_6C$. This transformation requires the interface

diffusion rather than volume diffusion of tungsten partition in M_7C_3. The reaction, although starting at the interface, is sometimes also called in situ [16,17]. As this reaction proceeds, most of the eutectic M_7C_3 carbides are eventually replaced by M_6C carbides. According to the EDX analysis, the stoichiometry of M_6C carbides varies between $W_{3.7}Cr_{1.2}Fe_{1.1}C$ and $W_{3.2}Cr_{1.4}Fe_{1.4}C$.

Fig. 6(a,b) are bright-field TEM micrographs illustrating plate-like $M_{23}C_6$ carbides precipitated around dislocations in the primary and eutectic austenite respectively. Fig. 6(c) shows SADP taken from an area covering $M_{23}C_6$ and the surrounding austenite with the same zone axis [010] in Fig. 6(a). Fig. 6(d) shows SADP of $M_{23}C_6$ carbides with a zone axis [138] in Fig. 6(b). Above $M_{23}C_6$ carbides are determined to be Cr–Fe-rich carbides using EDX.

Fig. 7(a,b) are bright-field TEM micrographs revealing small fibrous M_2C and needle-like MC carbides, respectively mainly nucleated at dense dislocations in the eutectic austenite. It is seen that fine M_2C and MC carbides are densely dispersed and their sizes are in a range from 10 to 20 nm.

Since the carbide precipitation is accompanied by a decrease in supersaturation, austenite will be destabilized and transform to martensite (α) during cooling. The martensite formed in the primary austenite is illustrated in Fig. 8.

The phase analyses of the as-tempered microstructure by X-ray diffraction are shown in Fig. 9, consistent with TEM results. Quantitative X-ray diffraction reveals that the volume fraction of austenite is about 21% in the peak-aged microstructure [11].

On the basis of the investigated results, the solidification and evolution sequence of phases in the coating can be represented as follows:

$$L \rightarrow \gamma + L \rightarrow \gamma + (\gamma + M_7C_3) \rightarrow (\gamma + M_{23}C_6 + M_2C + \alpha) + (\gamma + M_{23}C_6 + M_6C + M_2C + MC)$$

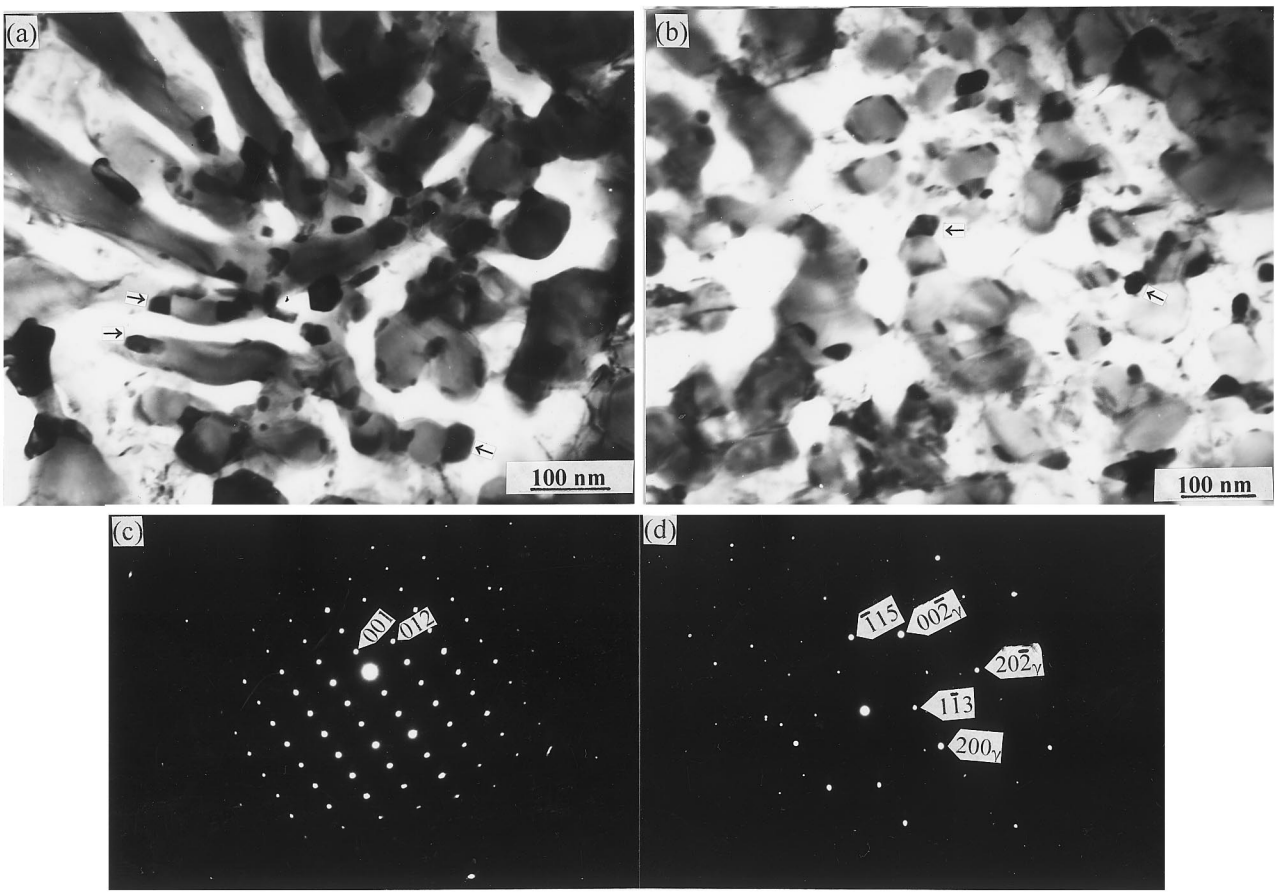

Fig. 5. TEM micrographs showing the in situ transformation of M_7C_3 to M_6C carbide: (a) and (b) bright-field images; (c) SADP of M_7C_3 with zone axis [100] in (a); (d) SADP of both M_6C carbide and γ-austenite with zone axes [110] and [010] respectively in (a) (all the arrows indicate M_6C carbides).

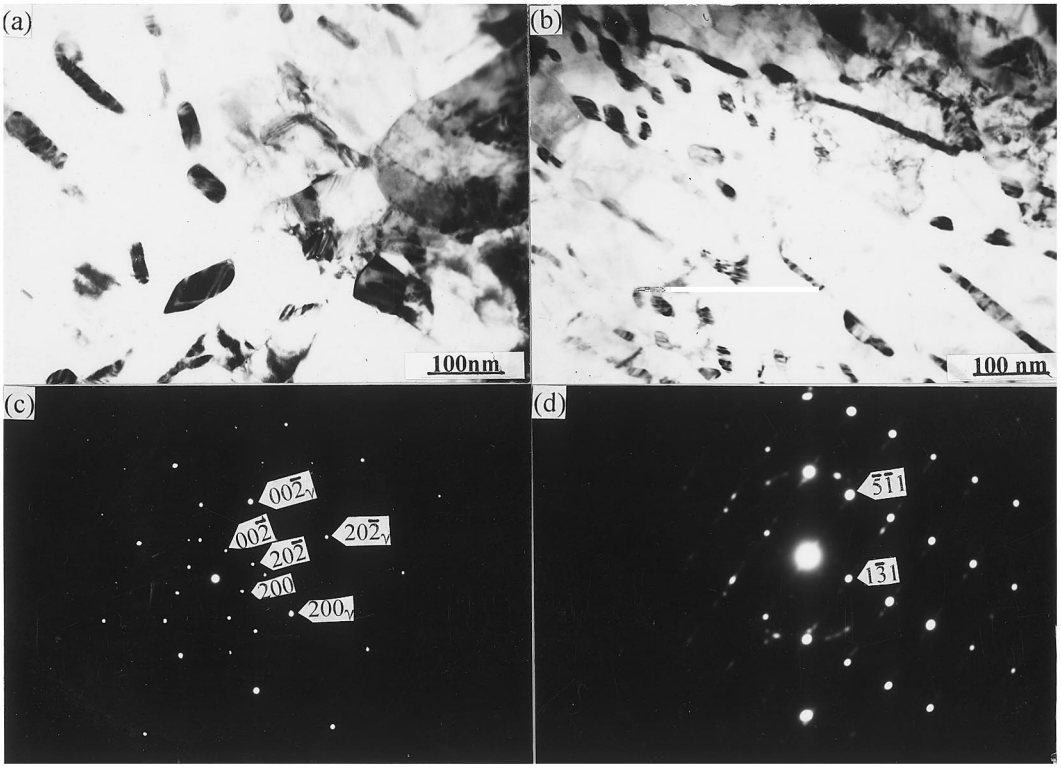

Fig. 6. TEM micrographs showing plate-like $M_{23}C_6$ carbides: (a) and (b) $M_{23}C_6$ carbides precipitated from the primary and eutectic austenite respectively; (c) SADP of $M_{23}C_6$ carbide and γ with the same zone axis [010] in (a); (d) SADP of $M_{23}C_6$ carbide with zone axis [138] in (b).

Fig. 7. TEM bright-field images showing M_2C (a) and MC (b) precipitated from eutectic austenite.

4. Conclusions

1. Laser-processed Fe–Cr–W–Ni–C alloy coatings were produced on a steel substrate using a 3 kW continuous wave CO_2 laser with 16 mm/s beam scanning speed, 3 mm beam diameter, 2 kW laser power, and 0.3 g/s feed rate.
2. The porosity and crack free coating was obtained with a maximum thickness of 730 μm, a microhardness of about 860 Hv, and a volumetric dilution ratio of about 6%.
3. The hypoeutectic microstructure comprising the primary dendritic γ-austenite and interdendritic eutectic consisted of γ-austenite and M_7C_3 carbide were formed. γ-Austenite was a non-equilibrium phase with extended solid solution of alloying elements.
4. High temperature tempering at 963 K promoted the precipitation of various carbides from nonequilibrium austenite and the evolution of M_7C_3 carbides. In situ carbide transformations existed of M_7C_3 to $M_{23}C_6$ and to M_6C carbide respectively mainly at M_7C_3/γ-austenite interfaces. In addition, the precipitation of $M_{23}C_6$, MC and M_2C carbides from austenite was also observed.